

Tropospheric Water Vapor and Climate Sensitivity

EDWIN K. SCHNEIDER, BEN P. KIRTMAN, AND RICHARD S. LINDZEN*

Center for Ocean–Land–Atmosphere Studies, Calverton, Maryland

(Manuscript received 8 August 1997, in final form 8 July 1998)

ABSTRACT

Estimates are made of the effect of changes in tropospheric water vapor on the climate sensitivity to doubled carbon dioxide (CO_2), using a coarse resolution atmospheric general circulation model coupled to a slab mixed layer ocean. The sensitivity of the model to doubled CO_2 is found as the difference between the equilibrium responses for control and doubled CO_2 cases. Clouds are specified to isolate the water vapor feedback. Experiments in which the water vapor distribution is specified rather than internally calculated are used to find the contribution of water vapor in various layers and latitude belts to the sensitivity.

The contribution of water vapor in layers of equal mass to the climate sensitivity varies by about a factor of 2 with height, with the largest contribution coming from layers between 450 and 750 mb, and the smallest from layers above 230 mb. The positive feedback on the global mean surface temperature response to doubled CO_2 from water vapor above 750 mb is about 2.6 times as large as that from water vapor below 750 mb. The feedback on global mean surface temperature due to water vapor in the extratropical free troposphere (above 750 mb) is about 50% larger than the feedback due to the lower-latitude free troposphere water vapor.

Several important sources of nonlinearity of the radiative heating rates were identified in the process of constructing the specified cloud and water vapor fields. These are (i) the interaction of clouds and solar radiation, which produces much more reflection of solar radiation for time mean clouds than for the instantaneous clouds; (ii) the correlation of clouds and water vapor, which produces less downward longwave radiation at the ground for correlated clouds and water vapor than when these fields are independent; and (iii) the interaction of water vapor with longwave radiation, which produces less downward longwave radiation at the ground for the average over instantaneous water vapor distributions than for the time mean water vapor distribution.

1. Introduction

Experiments were carried out with a GCM coupled to a slab mixed layer ocean to determine the contribution of the feedback from water vapor in various regions of the atmosphere on the sensitivity of global mean surface temperature to doubling of carbon dioxide (CO_2). While the boundary layer moisture is closely coupled to the underlying surface and can be considered, to a first approximation, to be near saturation at the local surface temperature, both advection and condensation play important roles in maintaining the water vapor distribution above the boundary layer, referred to in the following as free tropospheric water vapor (FTWV). It is well known that GCMs have major numerical difficulties and physical uncertainties in representing these processes

above the boundary layer; hence, it is important to estimate the magnitude of the FTWV feedback that may be affected by these numerical and physical problems.

The results from this study indicate that the water vapor feedback increases the model sensitivity by about a factor of 2, and that the contribution of FTWV is about 2.6 times larger than the feedback due to boundary layer moisture. The contribution of layers of equal mass to the sensitivity varies by about a factor of 2 with height, with the largest contribution per unit mass coming from layers between 450 and 750 mb, and the smallest from layers above 450 mb. Also, the contribution to the FTWV feedback from the extratropics (poleward of 30° latitude) is estimated to be 50% larger than the contribution from lower latitudes in our model.

The potential impact of the water vapor feedback on global warming was studied by Manabe and Strickler (1964) and Manabe and Wetherald (1967). They used a one-dimensional radiative convective equilibrium model with specified lapse rate and assumed that either specific humidity remained constant at all heights as the CO_2 concentration was increased, or that relative humidity remained constant. In the fixed relative humidity case, the specific humidity increases as the atmospheric temperature increases. The increase in specific humidity

* Current affiliation: Massachusetts Institute of Technology, Cambridge, Massachusetts.

Corresponding author address: Dr. Edwin K. Schneider, Center for Ocean–Land–Atmosphere Studies, 4041 Powder Mill Rd., Suite 302, Calverton, MD 20705-3106.
E-mail: schneide@cola.iges.org

increases the trapping of longwave radiation, further increasing the surface temperature, leading to a positive feedback and increased sensitivity. They found that the fixed relative humidity case was about a factor of 2 more sensitive to increased CO₂ than the case with fixed specific humidity.

The water vapor feedback in GCM simulations was studied by Mitchell et al. (1987) and by Mitchell and Ingram (1992). They used the technique of running the GCM radiation scheme diagnostically to find the change in the top of the atmosphere radiative fluxes when one quantity was changed to the value from a doubled CO₂ simulation with all other values held at the control experiment values. The quantities varied in the latter study were seasonal means, and included CO₂, surface albedo, water vapor, cloud, and surface and atmospheric temperature. This approach also does not include dynamical effects, as the sensitivity in each atmospheric column is found independently, and global mean values are found by spatial averaging.

The experiments presented here are analogous to those done by Manabe and Strickler (1964) and Manabe and Wetherald (1967), extending the previous studies by employing a GCM, with a full four-dimensional simulation of the heat fluxes, condensation, and radiation.

Although the importance of the FTWV feedback to global warming has been under discussion for some time (Lindzen 1990a,b; Betts 1990; Gates et al. 1992; Dickinson et al. 1995), there have been few modeling studies published that attempt to isolate and analyze this effect. Shine and Sinha (1991) examined the surface temperature response in a one-dimensional radiative/convective equilibrium model to 10% multiplicative changes in relative humidity in 50 mb thick atmospheric layers for various values of the solar constant meant to simulate the tropical, global average, and higher latitudes. They found a maximum response in the tropical case when the 50-mb layer centered at 800 mb is changed, and identified continuum absorption as an important contributor near the surface. They also found that the sensitivity in the tropical case was significantly larger than for the average case, and more than twice as large as for the higher-latitude case. They interpreted their results as indicating that water vapor near the surface could be important in providing a positive feedback even if the FTWV feedback was negative. Lindzen (1996) noted that the Shine and Sinha (1991) result is consistent with a strong influence of FTWV on surface temperature, since in the tropical case the regions above and below about 600 mb would contribute about equally to the surface warming for a vertically uniform increase of relative humidity. Spencer and Braswell (1997) pointed out that outgoing longwave radiation (OLR) is more sensitive to 3% additive changes (i.e., changing RH to RH + 3%) in upper-tropospheric layers (above 700–800 mb) than in lower layers of the atmosphere, a result that is also consistent with Shine and Sinha (1991) after

taking the considerations of Lindzen (1996) into account.

Here we address the question of the influence of water vapor feedback in different atmospheric layers in the vertical and in different horizontal regions, as in Shine and Sinha (1991), but in the context of a GCM. Our response from the different vertical layers resembles the results of Shine and Sinha (1991) but differs in that the higher-latitude FTWV feedback is more important in the GCM than the tropical feedback.

The surface temperature response to increased CO₂ involves important implicit contributions from the dynamics. The basic mechanism underlying the clear-sky greenhouse effect is that increasing absorber amounts changes the longwave optical properties of the atmosphere without changing the top of the atmosphere longwave or shortwave net radiative fluxes. The increased absorber amount causes the OLR to originate from a higher-tropospheric layer. Since the tropospheric temperature decreases with height, raising the emission level would cause reduced OLR if the temperature did not change. The temperature of the emitting layer must then rise to preserve the radiative balance. The reason that the atmospheric temperature must locally increase near the emission level when this level is raised by increasing the longwave absorber amount can be traced to the decrease of temperature with height. If the atmospheric temperature did not vary in the vertical, changing the emission level would have no effect on the energy balance, and no temperature change would be required. Similarly, if the atmospheric temperature increased with height near the emission level, then raising the emission level would result in a local decrease in temperature. This is the so-called lapse rate feedback. In low latitudes, the emitting layer is above 540 mb, while it descends to near 600 mb in high latitudes, as demonstrated by Fig. 1, which shows the effective emission level of the clear-sky OLR measured by the Earth Radiation Budget Experiment (Hurrell and Campbell 1992). Here the effective emission level is defined as the level at which the climatological annual mean tropospheric temperature is equal to the emission temperature, $(OLR/\sigma)^{1/4}$, where σ is the Stefan–Boltzmann constant. The temperature climatology used in this calculation was taken from the National Centers for Environmental Prediction (NCEP) reanalysis (Kalnay et al. 1996).

The effective emission level for the downward longwave radiation at the ground is analogously defined as the level at which the climatological annual mean tropospheric temperature is equal to $(DLB/\sigma)^{1/4}$, where DLB is the clear-sky downward longwave radiation at the bottom. This level was computed using NCEP reanalysis fluxes and temperatures and is also shown in Fig. 1. The effective emission level seen looking up from the surface is close to 800 mb in low latitudes and is near 600 mb in midlatitudes, similar to the behavior of the layer of maximum sensitivity found by Shine and Sinha (1991). In low latitudes, the layer responsible for

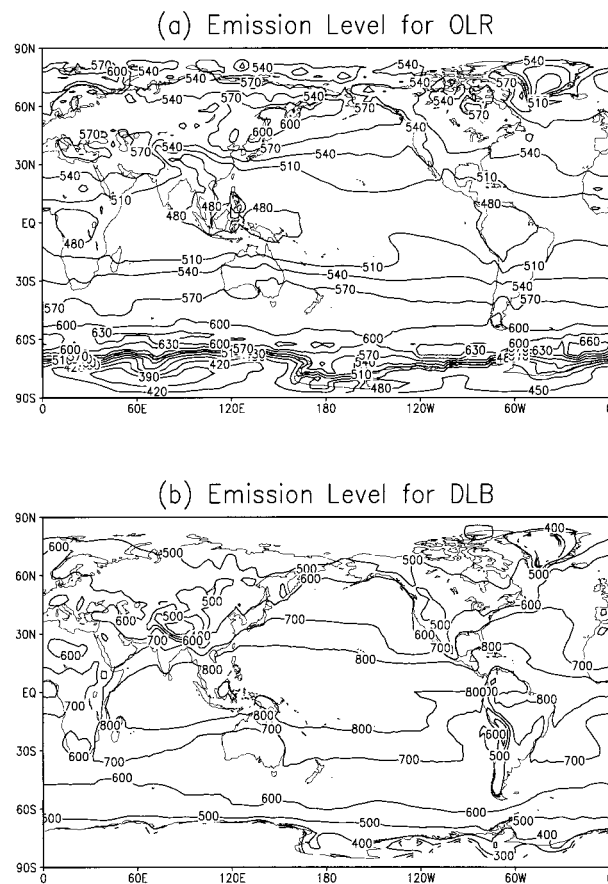


FIG. 1. (a) Effective emission level (in mb) for annual mean clear-sky OLR found using satellite OLR and temperature from the Kalnay et al. (1996) NCEP reanalysis (contour interval 30 mb). (b) Effective emission level (in mb) for clear-sky downward longwave radiation at the bottom of the atmosphere found using NCEP reanalysis (contour interval 100 mb).

most of the surface longwave radiative effect is far below the layer in which the temperature must change to balance the top of the atmosphere radiative budget. The direct response of the atmosphere to increased CO_2 is an increase in the upper-tropospheric temperature. The downward link to changes in the near-surface humidity and surface temperature is indirect, involving the interplay between atmospheric large-scale dynamics, moist convection, and radiation, and is not as easy to understand as the direct upper-tropospheric response.

Feedbacks involving FTWV and even upper-tropospheric water vapor can be important in modifying the surface response to increasing CO_2 . These feedbacks directly alter the upper-tropospheric temperature response near the emission level and also drive the surface response in a complex and indirect way. Increases are found in FTWV in GCM studies of the sensitivity to doubled CO_2 , with the relative humidity remaining nearly constant, as is commonly specified in one-dimensional studies such as Manabe and Wetherald (1967). This increase in FTWV increases the longwave optical

thickness, further raises the emission level, and causes a larger warming of upper-tropospheric temperature, amplifying the direct effect of increasing CO_2 .

The manner in which FTWV is maintained in nature and in models has not been fully documented and understood. Relevant studies include Salanthé and Hartmann (1997), who showed that the observed low-latitude upper-tropospheric humidity distribution is consistent with convective sources and radiatively induced subsidence along trajectories, and Del Genio et al. (1994), who analyzed the moisture budget of a GCM.

The simulation of FTWV is subject to purely numerical problems, as is evidenced by the common occurrence of unphysical negative values (Rasch and Williamson 1990), and there are large uncertainties in the parameterization of convective sources of water vapor (Lindzen 1990a,b; Betts 1990; Sun and Lindzen 1993).

It is currently believed that, equatorward of 30° latitude, the direct link between FTWV and the local underlying surface is through moist convection. Most of the air residing in the low-latitude upper troposphere was previously transported upward in convective clouds and then eventually sinks to the surface. In the low-latitude descending regions, air parcels conserve specific humidity, but relative humidity decreases because the temperature increases due to compression as the parcels descend (Sun and Lindzen 1993). Radiative cooling abates this temperature increase. Since most deep convection occurs close to the equator, in the intertropical convergence zone (ITCZ) over the ocean and in contiguous land regions, the last contact the air in the low-latitude upper troposphere has with the surface is in the regions of warmest SST. An air parcel may travel many thousands of kilometers horizontally as it subsides. The water vapor distribution above the boundary layer in the dry subsidence regions is then not directly related to underlying local surface conditions and is controlled by the large-scale dynamics that connects these areas to the regions of moist convection. The importance of horizontal transports by atmospheric dynamics complicates the simple one-dimensional picture of the water vapor feedback presented by Manabe and Strickler (1964) and Manabe and Wetherald (1967), potentially decoupling the near-surface and upper-tropospheric responses.

Apart from the summer season, FTWV in the extratropics is thought to be maintained primarily by the balance between quasi-horizontal large-scale advection and large-scale condensation. Both of these processes occur on the resolved scales of the GCM. Despite the greater confidence in the ability of the GCM to accurately simulate the important physical processes of the water budget in the extratropics than in the Tropics, numerical problems with negative specific humidity are most common in the Northern Hemisphere extratropics in association with steep topography. Given that the GCM simulation in both latitude regimes is uncertain, but for different reasons, we examine the sensitivity to

the FTWV feedback separately in the Tropics and extratropics.

The experimental design uses specified clouds and eliminates the sea ice albedo feedback in order to better isolate the water vapor feedback. Some technical choices are also made in order to reduce cloud/shortwave and water vapor/longwave nonlinearities found when cloud and water vapor are specified. However, neither a cloud/water vapor/longwave nonlinearity nor snow albedo and cloud temperature feedbacks are eliminated.

2. Experiments

The model and experimental design are described in this section. The techniques for specifying the clouds and water vapor are also explained.

a. The model

The model is a low-resolution atmospheric GCM coupled at the lower boundary to a 50 m deep slab mixed layer ocean and a land model with a realistic distribution of surface properties. Horizontal ocean heat fluxes are zero, and there is no specified or parameterized sea ice, so that the sea ice albedo feedback is eliminated. The slab mixed layer ocean is commonly used in GCM estimates of climate sensitivity (Mitchell et al. 1990). The atmospheric model was developed from the National Meteorological Center (now the National Centers for Environmental Prediction) medium-range forecast model, circa 1986 (Sela 1980). The model is described by Schneider and Kinter (1994) and was employed by Lindzen et al. (1995) and Schneider et al. (1997). The model is spectral with rhomboidal 15 horizontal resolution and nine levels in the vertical and includes a full suite of physical parameterizations. The distribution of levels in the vertical is taken to be the same as that of the Geophysical Fluid Dynamics Laboratory atmospheric GCM (Gordon and Stern 1982), a model that has been used in many studies of the greenhouse effect.

The primary effects being investigated here are the influences of CO₂ and water vapor on longwave radiation in the context of a GCM. The influence of these constituents on the longwave radiative transfer is modeled using the scheme of Harshvardhan et al. (1987), which includes the effects of the water vapor continuum. Other radiative parameterizations are for shortwave radiative transfer (Lacis and Hansen 1974; Davies 1982) and cloud amounts for cloud-radiative interactions (Slingo 1987). Shortwave radiative calculations are performed every 3 simulated hours, and longwave computations are performed at 6-hourly intervals. The solar forcing varies both annually and diurnally. A climatological ozone distribution is specified. The parameterization of moist convection is based on the scheme proposed by Kuo (1965).

b. Experimental design

The experiments are designed to isolate the contribution of water vapor to the sensitivity of the GCM to doubled CO₂. The technique adopted is to compare the model sensitivity when the water vapor seen by the radiative calculations is unconstrained to that when the water vapor in various regions is specified.

The sensitivity of the unconstrained model to doubled CO₂ is found by taking the difference between equilibrium 1 × CO₂ (345 ppmv) and 2 × CO₂ (690 ppmv) simulations. The CO₂ concentrations differ slightly from the values that have usually been chosen for such studies (300 and 600 ppmv). Results from the unconstrained sensitivity experiments have been reported in Schneider et al. (1997). The three-dimensional cloud and water vapor distributions supplied to the radiation routines are saved every 3 h for separate 1-yr periods of the unconstrained 1 × CO₂ and 2 × CO₂ simulations.

1) SPECIFICATION OF CLOUDS

Since the object of the study is to evaluate the water vapor feedback, cloud radiative feedbacks are suppressed by specifying the cloud distribution. An annual cloud dataset was created by saving the instantaneous cloud distribution each time the radiative calculations were performed for a year of the unconstrained simulation. The cloud distribution is retrieved from the dataset for the corresponding hour of the year and used in the calculation of the radiative heating. This rather cumbersome procedure both reduces the cloud feedback effects on the model sensitivity and gives cloud radiative interactions similar to those in the unconstrained simulations.

Experiments were initially made with time mean specified cloudiness (monthly or daily) saved from the unconstrained sensitivity simulations. However, the cloud-shortwave interaction was found to be strongly nonlinear. When monthly mean clouds were used, the top of the atmosphere-reflected shortwave radiation was much larger than for the unconstrained simulations, by up to 80 W m⁻² in the zonal mean at summer hemisphere latitudes. On the other hand, the longwave radiation was not affected nearly as much by the use of monthly mean clouds. The reduction of absorbed solar radiation led to a rapid decrease in global mean surface temperature in the 1 × CO₂ case with 1 × CO₂ monthly clouds prescribed (3°C in the first year). The use of daily mean clouds also led to an unacceptably large increase in the reflected solar radiation relative to the unconstrained simulations. To solve the problem of nonlinear cloud-shortwave interactions, the local instantaneous cloud distributions from an arbitrarily chosen year were used, producing results close to those of the unconstrained simulations. A similar method for specifying various fields (clouds, sea ice, water vapor, lapse rate, and

ground temperature) in climate sensitivity studies with a GCM was used by Hansen et al. (1997).

In order to model different optical properties for water and ice, cloud emissivity is taken to be a function of temperature, with emissivity increasing as temperatures near 250 K increase. The cloud feedback is not completely eliminated by specifying cloud amounts, since the cloud temperature is not specified. This feedback can be detected and will be mentioned below.

2) SPECIFICATION OF WATER VAPOR

The specification of water vapor for the radiative calculations uses the same approach as is adopted for the clouds. An annual water vapor dataset was created by saving the instantaneous water vapor distribution each time the radiative calculations were performed for a year of the unconstrained simulation. The year from which the water vapor was saved was not the same as the year from which the clouds were saved, so that the specified clouds and water vapor are not directly related to each other. The water vapor is retrieved from the dataset for the corresponding hour of the year and used instead of the water vapor determined internally by the model in the calculation of the shortwave and longwave radiative heating. Outside of the region of specification, the water vapor distribution as internally generated by the GCM is supplied to the radiative calculations.

The prognostic equation for water vapor is not altered, nor are the sources and sinks of water vapor due to the physical parameterizations of condensation, precipitation, evaporation, or diffusion. Calculations involving water vapor then use a combination of a specified water vapor distribution for radiative calculations in certain regions and the prognostic value for all other calculations.

As with the clouds, the motivation for the use of instantaneous rather than time mean water vapor was to eliminate a nonlinearity in the model response. With specified $1 \times \text{CO}_2$ clouds, the use of monthly mean specified water vapor led to an increase of about 0.5°C in the equilibrium global mean surface temperature relative to the case with unconstrained water vapor. The same effect occurred when daily mean specified water vapor was used. This effect is eliminated by specifying water vapor snapshots.

3. Results

The results from the sensitivity experiments are summarized in Table 1. In each case, the sensitivity is found as the difference between two GCM simulations carried out to quasi equilibrium. The values given for the sensitivity are estimates from 5-yr averages of global mean temperature difference after the simulations appear to have reached a climatic equilibrium. There is significant interannual variability in the global mean temperatures, so that the sensitivity estimates are uncertain by $\pm 0.1^\circ\text{C}$.

TABLE 1. Sensitivity of global mean surface temperature to doubled CO_2 . Each sensitivity is the difference between a $1 \times \text{CO}_2$ and a $2 \times \text{CO}_2$ simulation.

Experiment	Sensitivity ($^\circ\text{C}$)
Unconstrained cloud and water vapor	2.30
Unconstrained water vapor ^a	1.98
Specified water vapor everywhere ^b	2.05
Specified water vapor everywhere ^c	1.08
Specified water vapor above 750 mb ^c	1.24
Specified water vapor above 450 mb ^c	1.57
Specified water vapor above 230 mb ^c	1.77
Specified water vapor above 750 mb, equatorward of 30°C ^c	1.67
Specified water vapor above 750 mb, poleward of 30°C ^c	1.50

^a Specified cloud from unconstrained $1 \times \text{CO}_2$ simulation.

^b Specified cloud from unconstrained $1 \times \text{CO}_2$ simulation; specified water vapor from the unconstrained $2 \times \text{CO}_2$ simulation in $2 \times \text{CO}_2$ case, and from the $1 \times \text{CO}_2$ simulation in $1 \times \text{CO}_2$ case.

^c Specified cloud and water vapor from unconstrained $1 \times \text{CO}_2$ simulation.

a. Unconstrained cloud and water vapor

The sensitivity of the global mean surface temperature to doubled CO_2 is 2.3°C for the unconstrained model. This sensitivity is smaller than that which would be found if sea ice were calculated and the positive feedback from the ice albedo effect included. As noted in Schneider et al. (1997) there is a net global mean top of the atmosphere radiative imbalance (shortwave absorbed minus longwave emitted) in equilibrium of 2.5 W m^{-2} , which is balanced by a corresponding imbalance in the land surface energy budget. This imbalance does not vary strongly from simulation to simulation and does not affect the sensitivity.

The difference in the annual and zonal mean specific and relative humidity, and the fractional changes in specific humidity associated with doubling CO_2 are shown in Fig. 2. The specific humidity difference is positive everywhere below 100 mb, with much larger increases in the lower troposphere than in the upper troposphere. The total increase in precipitable water is 4.6 mm, of which 2.7 mm occurs below 750 mb. The fractional change in the specific humidity is largest, exceeding 30%, throughout the high-latitude troposphere and in the tropical upper troposphere, and becomes smaller at low levels in the Tropics. The fractional change in relative humidity is small, and the relative humidity is nearly the same in the unconstrained $1 \times \text{CO}_2$ and $2 \times \text{CO}_2$ simulations, as is commonly found in GCMs and assumed in one-dimensional models.

The zonal mean atmospheric temperature near the equator increases by 3.2°C at 250 mb and by 2.2°C at the surface, following the change in the moist adiabat in the warmer climate. This decrease in the lapse rate indicates a negative feedback, at least in the tropical troposphere near the emission level, by the lapse rate feedback mechanism. The global mean temperature

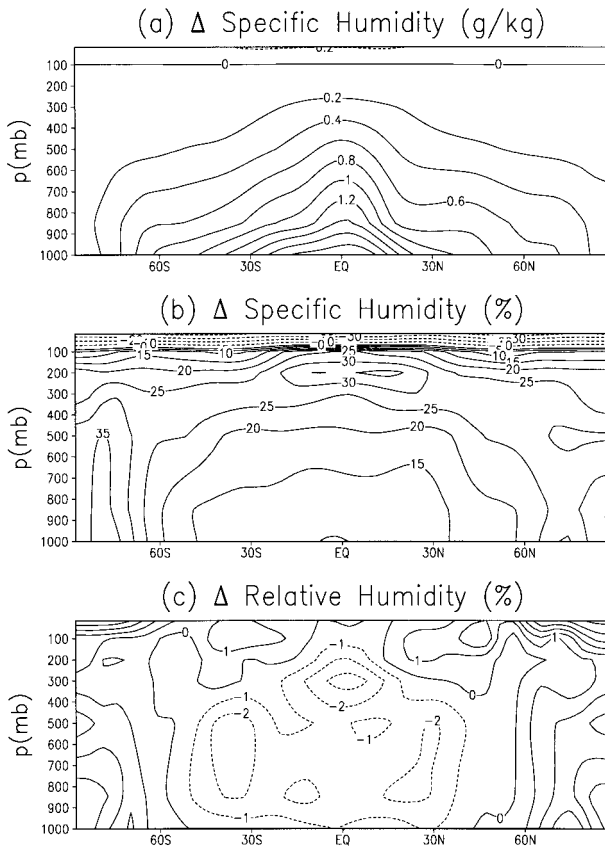


FIG. 2. Changes in zonal means as a function of latitude and pressure in the unconstrained simulations, $2 \times \text{CO}_2$ minus $1 \times \text{CO}_2$; (a) specific humidity, contour interval 0.2 g kg^{-1} ; (b) percentage change in specific humidity, contour interval 5% for positive (solid) contours and 10% for negative (dashed) contours; (c) relative humidity, contour interval 1%.

change is more nearly uniform with height, as shown in Lindzen et al. (1995, Fig. 3).

b. Specified clouds and unconstrained water vapor

The clouds from the unconstrained $1 \times \text{CO}_2$ simulation were specified and water vapor was unconstrained. The sensitivity to doubled CO_2 in this experiment was 1.98°C . The decrease in sensitivity from the unconstrained case can be attributed to the elimination of the cloud feedback. The reduction in the cloud feedback results from a 0.7 W m^{-2} reduction in the global mean absorbed solar radiation in the $2 \times \text{CO}_2$ simulation with fixed clouds, relative to the unconstrained $2 \times \text{CO}_2$ simulation.

Specification of the cloud amounts allows some other shortwave radiative feedbacks to be easily seen. This is illustrated by the annual mean difference in absorbed shortwave between the $1 \times \text{CO}_2$ and $2 \times \text{CO}_2$ simulations with specified clouds, shown in Fig. 3. The increase in shortwave absorption in higher latitudes when CO_2 is doubled is due to a snow albedo feedback, with snow accumulating later and melting sooner in the extratropics in the warmer climate. The annual and zonal mean increase in solar radiation absorbed accounted for by the snow albedo feedbacks reaches about 0.5 W m^{-2} in some extratropical latitude bands.

In the global mean, the increase in solar radiation absorption due to the snow albedo feedback is very nearly compensated for by a reduction due to increased reflection by clouds, noticeable in Fig. 3 in low latitudes. This increased reflection with fixed cloud amount is due to the assumed temperature dependence of the cloud emissivity. Cloud amount is fixed, but cloud temperature changes in the sensitivity experiments. The effect is

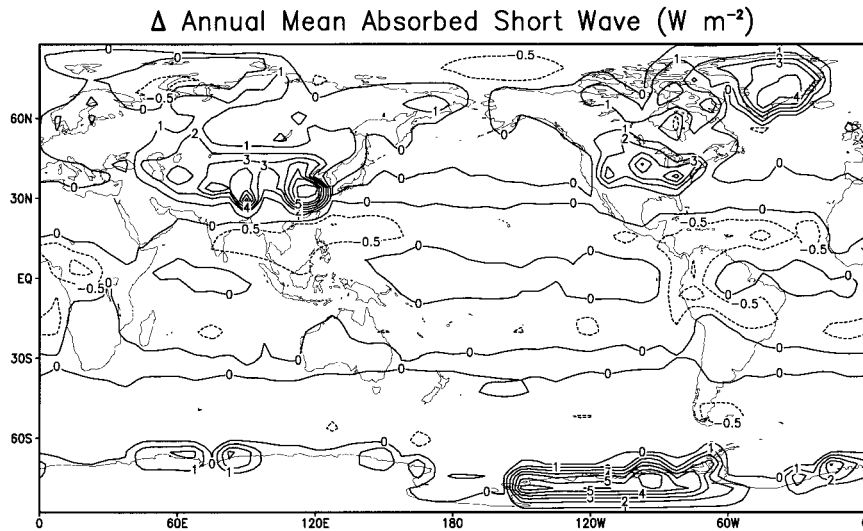


FIG. 3. Change in annual mean solar radiation absorbed by the atmosphere and surface in the simulations with specified cloud and unconstrained water vapor, $2 \times \text{CO}_2$ minus $1 \times \text{CO}_2$; contour interval 1 W m^{-2} , with an additional contour at -0.5 W m^{-2} .

largest in the subtropics rather than the ITCZ, because the high clouds in the ITCZ remain below the transition temperature. Due to coincidental compensation between the snow albedo feedback and the cloud temperature feedback, the global mean change in the absorbed solar radiation is less than 0.1 W m^{-2} in the sensitivity experiments when clouds are specified, and the snow and cloud effects will be not be considered in the feedback analysis of section 4.

The global mean surface temperature of the $1 \times \text{CO}_2$ simulation with specified clouds is 0.4°C higher than the global mean surface temperature of the corresponding simulation with unconstrained clouds. This surface warming occurs despite the fact that the specified and unconstrained clouds have nearly the same effects on the top of the atmosphere and surface shortwave fluxes. Examination of the surface energy budget indicates that the warming is due to a nonlinear longwave interaction between the clouds and the water vapor. In the unconstrained simulation, clouds and water vapor are strongly positively correlated by assumption. However, in the simulation with fixed clouds, this correlation is reduced, since the clouds are no longer directly determined from the water vapor. Therefore, longwave opacity is increased in clear areas in the specified cloud simulation, by increased water vapor. However, the longwave opacity is already large in the cloudy areas, and reducing the water vapor in these regions has little effect. The net effect of the decorrelation of the clouds and water vapor is then a surface warming.

c. Specified clouds and water vapor

The prescribed specific humidity is calculated from the unconstrained simulation with $2 \times \text{CO}_2$ in the $2 \times \text{CO}_2$ simulation. Similarly, the prescribed specific humidity in the $1 \times \text{CO}_2$ simulation is calculated from the unconstrained simulation with $1 \times \text{CO}_2$. Both simulations use the $1 \times \text{CO}_2$ -specified clouds. The sensitivity in this experiment is found to be 2.05°C . The feedback analysis in section 4 will use this as the value for the sensitivity to doubled CO_2 with the full water vapor feedback.

Preliminary experiments used the monthly mean of the specific humidity from the unconstrained simulation, and specified clouds. The $1 \times \text{CO}_2$ global mean surface temperature was 0.5°C warmer than the simulation with unconstrained water vapor. A similar relative warming was also found when the specific humidity was interpolated from daily mean values of the unconstrained control. Specifying instantaneous values, as done with the clouds, eliminates this nonlinear warming effect, and the effect is analogous to the cloud/water vapor/longwave radiation nonlinearity described above. When water vapor is unconstrained, the instantaneous specific humidity varies strongly horizontally, but has relatively high vertical correlation. When time mean values are

used, the radiative balance is affected less in moist than in dry regions and leads to surface warming.

d. Specified water vapor in the free troposphere and upper troposphere

When the $1 \times \text{CO}_2$ water vapor is specified everywhere, the sensitivity is found to be 1.08°C . Sensitivity of 1.24°C is found for water vapor specified in the free troposphere (pressure <750 mb) and unconstrained below that level. The sensitivity is also found for two cases of water vapor specified in the upper troposphere. When the region of specified water vapor is taken to be pressure <450 mb, the sensitivity is 1.57°C . The sensitivity is 1.77°C when the region of specified water vapor is taken to be pressure <230 mb.

The vertical structure of the global mean atmospheric temperature sensitivity for the cases of different vertical regions of water vapor specification is shown in Fig. 4a. In all cases, the temperature increases almost uniformly with height for pressure greater than 300 mb. The mean tropospheric lapse rate below 300 mb is not affected by the details of the water vapor feedback in the vertical. The stratospheric cooling found for pressure less than 100 mb is also independent of the water vapor feedback.

The horizontal structure of the zonal mean surface temperature sensitivity for the cases of different vertical regions of water vapor specification is shown in Fig. 5a. As the water vapor feedback is allowed in deeper layers, the sensitivity increases at all latitudes, with some exceptions near the poles. Also, the sensitivity at the higher latitudes increases by a larger amount than the sensitivity near the equator.

e. Latitudinally specified water vapor

When water vapor is specified in the low-latitude free troposphere between 30°S and 30°N , the sensitivity is found to be 1.67°C . The sensitivity decreases to 1.5°C when FTWV is specified in the latitudes more than 30° from the equator.

The vertical structure of the sensitivity for these cases, relative to the sensitivity with unconstrained water vapor, is shown in Fig. 4b. The sensitivity to the low-latitude water vapor feedback is comparatively more important than the higher-latitude feedback in the upper layers, while the water vapor feedback in the extratropics is more important than the low-latitude water vapor feedback near the surface. This behavior contrasts with that shown in Fig. 4a where the curves do not cross below 100 mb. Following the discussion in the introduction, the lapse rate feedback is then reduced by low-latitude FTWV feedback and increased by higher-latitude FTWV feedback.

The horizontal structure of the sensitivity for the meridional specification experiments is shown in Fig. 5b. The sensitivity in the Tropics is larger, and the higher-

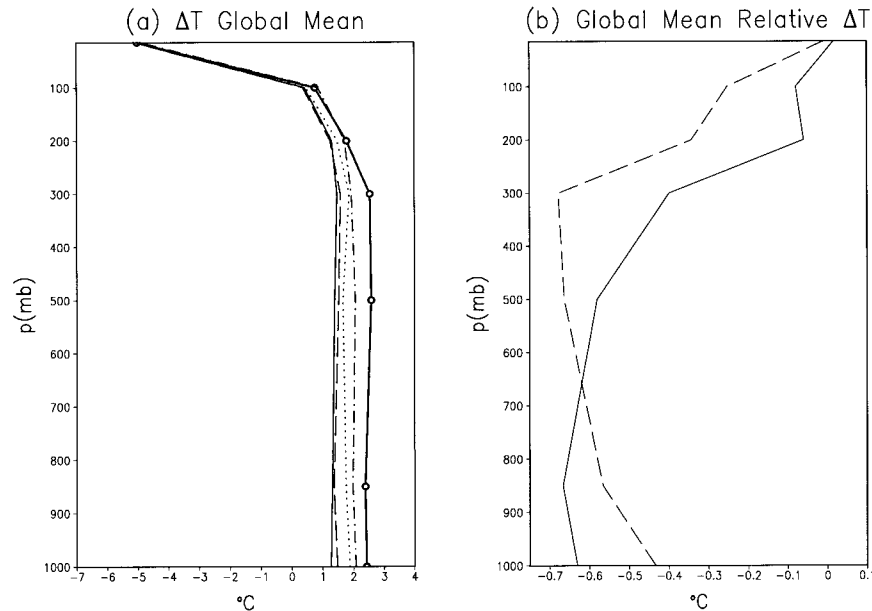


FIG. 4. Global mean atmospheric temperature sensitivity to doubled CO₂ as a function of pressure with specified clouds. (a) The 1 × CO₂ water vapor specified in different regions in the vertical: nowhere (dark solid with open circles), everywhere (thin solid), above 750 mb (long dashed), above 450 mb (dotted), above 230 mb (dash-dot). (b) The 1 × CO₂ water vapor specified in different regions in the horizontal above 750 mb: latitudes more than 30° from the equator (solid); within 30° latitude of the equator (dashed).

latitude sensitivity is smaller, in the experiment where water vapor is specified poleward of 30° than when it is specified equatorward of 30°. The effect of the horizontal heat transports can be evaluated by taking the difference of the sensitivity from the cases with meridionally restricted feedback from the sensitivity with the FTWV feedback eliminated globally. When the water vapor is specified equatorward of 30°, the horizontal heat transports warm the tropical surface temperature by about 0.2°C. When the water vapor is specified poleward of 30°, the effect of the horizontal heat transports on the midlatitude sensitivity is small but leads to similar sensitivity near the poles as in the case when water vapor is specified equatorward of 30°.

4. Feedback analysis

The sensitivities obtained in the experiments reported in Table 1 are used to infer feedback factors. These feedback factors can then be compared to determine the relative importance of the water vapor feedbacks in different regions, and to predict the behavior of the model in the presence of other feedbacks. The feedback analysis follows Hansen et al. (1984) and Schlesinger and Mitchell (1987). The response equation, which is obtained by linearizing the top of the atmosphere energy balance, is

$$\Delta T_s = \frac{g}{1 - \sum_i f_i}, \quad (1)$$

where ΔT_s is the global mean surface temperature sensitivity, g is the response to ΔCO_2 in the absence of other feedbacks, and f_i are the feedback factors. Although the feedback factors add together to determine the total feedback, the sensitivities to the different feedbacks are not additive due to the nonlinearity of (1), when any one of, or the sum of, the feedback factors in the denominator of (1) is not small compared to one.

The feedback factors are estimated from the responses in the various sensitivity experiments, using (1) and the results given in Table 1. The value used for the gain is $g = 1.08^\circ\text{C}$ from the experiment with specified 1 × CO₂ water vapor everywhere. The additive property is used to find the feedback factors for the various layers, regions, and for the clouds. The resulting feedback factors are shown in Table 2. The feedback factors for various combinations of these regions may be found by addition. The feedback factor for water vapor in the whole atmosphere is 0.47, of which the free troposphere contributes 0.34. The feedback factor from the higher-latitude FTWV feedback is somewhat larger than that for the low-latitude FTWV feedback.

Estimates of the feedback factors per 100 mb are also shown in Table 2 for the various layers. The largest contribution to the water vapor feedback per unit mass is found to come from the lower free troposphere, 750 mb < p < 450 mb, with contributions from the surface layer about 80% as strong, and contributions about 60% as strong from $p < 450$ mb.

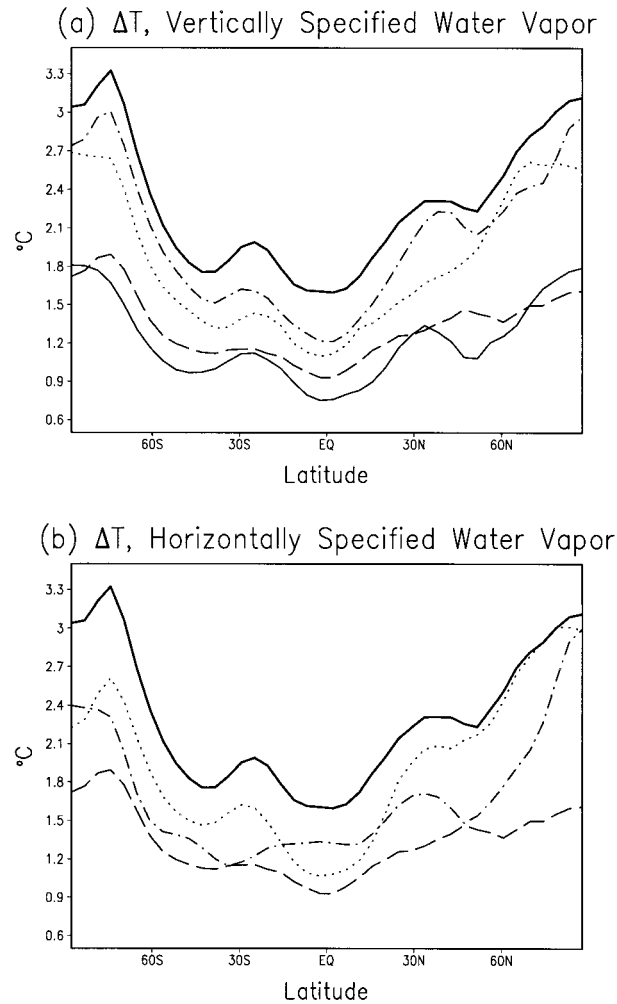


FIG. 5. Zonal mean surface temperature sensitivity to doubled CO_2 as a function of latitude with specified clouds. (a) The $1 \times \text{CO}_2$ water vapor specified in different regions in the vertical: nowhere (dark solid), everywhere (thin solid), above 750 mb (long dashed), above 450 mb (dotted), above 230 mb (dash-dot). (b) The $1 \times \text{CO}_2$ water vapor specified in different regions in the horizontal above 750 mb: latitudes more than 30° from the equator (dashed-dot); within 30° latitude of the equator (dotted). For comparison, the results with unconstrained water vapor (dark solid) and water vapor specified globally above 750 mb (long dashed) are also shown.

5. Summary

Numerical experiments were conducted to estimate the magnitude of the feedback due to tropospheric water vapor on the sensitivity of global mean surface temperature to doubled CO_2 . An atmospheric GCM coupled to a 50-m slab mixed layer ocean, with no horizontal ocean heat flux and no sea ice, was used. The model had realistic distributions of land, sea, and orography. The forcing was provided by annually and diurnally varying incident solar radiation. The relative humidity in the GCM remained approximately constant in the unconstrained sensitivity to doubled CO_2 .

In order to concentrate on the water vapor feedback,

TABLE 2. Feedback factor contributions from water vapor in various regions and from clouds.

Parameter	Feedback factor	Feedback factor $(100 \text{ mb})^{-1}$
Boundary layer water vapor ($1014 \text{ mb} < p < 750 \text{ mb}$)	0.13	0.049
Lower free tropospheric water vapor ($750 \text{ mb} < p < 450 \text{ mb}$)	0.18	0.06
Middle free tropospheric water vapor ($450 \text{ mb} < p < 230 \text{ mb}$)	0.08	0.036
Upper free tropospheric water vapor ($p > 230 \text{ mb}$)	0.08	0.034
Free tropospheric water vapor, latitudes within 30° of equator	0.15	—
Free tropospheric water vapor, latitudes outside of 30° from equator	0.22	—
Clouds	0.06	—

cloud feedbacks were reduced by specifying cloud amounts. This procedure did not eliminate a small negative cloud shortwave feedback due to temperature dependence of cloud properties, but that feedback was almost entirely compensated for in the global and annual mean by a positive snow albedo feedback. The specified cloud amounts were chosen to be annually repeating instantaneous values from a year of an unconstrained $1 \times \text{CO}_2$ simulation. This procedure was used to eliminate a nonlinear feedback where specifying the monthly or daily means of the clouds from the unconstrained simulation led to a much larger reflection of solar radiation than the time mean of the reflection from the instantaneous clouds.

A similar procedure of specification of annually repeating instantaneous values from the unconstrained integration was used for the water vapor, in order to eliminate the water vapor feedback. The use of instantaneous values eliminated another nonlinear feedback, in which specification of monthly mean water vapor led to a 0.5°C increase in the global mean surface temperature. This nonlinearity results from decorrelation of water vapor in the vertical due to time averaging, leading to enhanced longwave blocking.

A third nonlinear feedback that was found, due to specifying cloud and water from different years of the unconstrained integration, was not eliminated. This nonlinearity raised the surface temperature by 0.4°C due to decorrelation of water vapor and clouds, leading to increased blocking of longwave radiation. It is expected that the procedure of comparing the $1 \times \text{CO}_2$ and $2 \times \text{CO}_2$ simulations, both with the same regions of specified water vapor, suppresses the effect of the radiative nonlinearities on the sensitivity estimates.

The total water vapor feedback factor was 0.47, which is similar to the estimate of the water vapor feedback by Manabe and Strickler (1964) and Manabe and Wetherald (1967). The water vapor feedback from the free troposphere was found to be 2.6 times as large as that from the near-surface layer. Almost half of the FTWV

feedback is due to water vapor above 450 mb. The results on the contributions from the vertical layers appear to be consistent with those of Shine and Sinha (1991), when the layer depths are taken into account.

The feedback due to FTWV from latitudes greater than 30° from the equator was found to be 1.5 times as large as the feedback due to FTWV from within 30° latitude of the equator. The higher latitudes were also the regions of largest percentage change in the specific humidity. The results of Shine and Sinha (1991) appear to give a different picture, with the low-latitude feedback larger than the higher-latitude feedback. However, as the relative increase in FTWV was about three times larger in the GCM than taken in the one-dimensional model, it is possible that with suitable scaling the results of both studies are consistent.

Acknowledgments. B. P. Kirtman and E. K. Schneider acknowledge support from NSF Grant ATM-9321354, NOAA Grant NA46GP0217, and NASA Grant NAGW5213. E. K. Schneider was also supported by NSF Grant ATM-9520579. R. S. Lindzen's efforts were supported by Grants 914441-ATM from the National Science Foundation, NAG5-6304 from the National Aeronautics and Space Administration, and DE-FG02-93ER61673 from the Department of Energy. We thank Jim Kinter, Uma Bhatt, and anonymous reviewers for useful suggestions.

REFERENCES

- Betts, A. K., 1990: Greenhouse warming and the tropical water budget. *Bull. Amer. Meteor. Soc.*, **71**, 1464–1465.
- Davies, R., 1982: Documentation of the solar radiation parameterization in the GLAS climate model. NASA Tech. Memo. 83961, 57 pp. [Available from NASA Center for Aerospace Information, Attn: STI Ordering Service, 7121 Standard Dr., Hanover, MD 21076-1320; available online from www.sti.nasa.gov.]
- Del Genio, A. D., W. Kovari Jr., and M.-S. Yao, 1994: Climatic implications of the seasonal variation of upper tropospheric water vapor. *Geophys. Res. Lett.*, **21**, 2701–2704.
- Dickinson, R. E., V. Meleshko, D. Randall, E. Sarachik, P. Silva-Dias, and A. Slingo, 1995: Climate processes. *Climate Change 1995: The Science of Climate Change*, J. T. Houghton, L. G. Meira Filho, B. A. Callander, N. Harris, A. Kattenberg, and K. Maskell, Eds., Cambridge University Press, 193–227.
- Gates, W. L., J. F. B. Mitchell, G. J. Boer, U. Cubasch, and V. P. Meleshko, 1992: Climate modelling, climate prediction and model validation. *Climate Change 1992: The Supplementary Report to the IPCC Scientific Assessment*, J. T. Houghton, B. A. Callander, and S. K. Varney, Eds., Cambridge University Press, 97–134.
- Gordon, C. T., and W. F. Stern, 1982: A description of the GFDL global spectral model. *Mon. Wea. Rev.*, **110**, 625–644.
- Hansen, J., A. Lacis, D. Rind, G. Russell, P. Stone, I. Fung, R. Ruedy, and J. Lerner, 1984: Climate sensitivity: Analysis of feedback effects. *Climate Processes and Climate Sensitivity*, *Geophys. Monogr.*, No. 29, Amer. Geophys. Union, 130–163.
- , M. Sato, and R. Ruedy, 1997: Radiative forcing and climate response. *J. Geophys. Res.*, **102**, 6831–6864.
- Harshvardhan, R. Davies, D. A. Randall, and T. G. Corsetti, 1987: A fast radiation parameterization for atmospheric circulation models. *J. Geophys. Res.*, **92** (D1), 1009–1016.
- Hurrell, J. W., and G. G. Campbell, 1992: Monthly mean global satellite data sets available in CCM history tape format. NCAR Tech. Rep. NCAR/TN-371+STR, 94 pp. [Available from National Center for Atmospheric Research, P.O. Box 3000, Boulder, CO 80307.]
- Kalnay, E., and Coauthors, 1996: The NCEP/NCAR 40-Year Reanalysis Project. *Bull. Amer. Meteor. Soc.*, **77**, 437–471.
- Kuo, H. L., 1965: On the formation and intensification of tropical cyclones through latent heat release by cumulus convection. *J. Atmos. Sci.*, **22**, 40–63.
- Lacis, A. A., and J. E. Hansen, 1974: A parameterization for the absorption of solar radiation in the earth's atmosphere. *J. Atmos. Sci.*, **31**, 118–133.
- Lindzen, R. S., 1990a: Some coolness concerning global warming. *Bull. Amer. Meteor. Soc.*, **71**, 288–299.
- , 1990b: Greenhouse warming and the tropical water budget: Response. *Bull. Amer. Meteor. Soc.*, **71**, 1465–1467.
- , 1996: The importance and nature of the water vapor budget in nature and models. *Climate Sensitivity to Radiative Perturbations: Physical Mechanisms and Their Validation*, H. Le Treut, Ed., NATO ASI Series, Vol. IX, Springer-Verlag, 51–66.
- , B. Kirtman, D. Kirk-Davidoff, and E. K. Schneider, 1995: Seasonal surrogates for climate. *J. Climate*, **8**, 1681–1684.
- Manabe, S., and R. F. Strickler, 1964: Thermal equilibrium of the atmosphere with convective adjustment. *J. Atmos. Sci.*, **21**, 361–385.
- , and R. T. Wetherald, 1967: Thermal equilibrium of the atmosphere with a given distribution of relative humidity. *J. Atmos. Sci.*, **24**, 241–259.
- Mitchell, J. F. B., and W. J. Ingram, 1992: Carbon dioxide and climate: Mechanisms of changes in cloud. *J. Climate*, **5**, 5–21.
- , C. A. Wilson, and W. M. Cunningham, 1987: On CO₂ climate sensitivity and model dependence of results. *Quart. J. Roy. Meteor. Soc.*, **113**, 293–322.
- , S. Manabe, T. Tokioka, and V. Meleshko, 1990: Equilibrium climate change. *Climate Change: The IPCC Scientific Assessment*, J. T. Houghton, G. J. Jenkins, and J. J. Ephraums, Eds., Cambridge University Press, 131–172.
- Rasch, P. J., and D. L. Williamson, 1990: Computational aspects of moisture transport in global models of the atmosphere. *Quart. J. Roy. Meteor. Soc.*, **116**, 1071–1090.
- Salanthe, E. P., and D. L. Hartmann, 1997: A trajectory analysis of tropical upper-tropospheric moisture and convection. *J. Climate*, **10**, 2533–2547.
- Schlesinger, M. E., and J. F. B. Mitchell, 1987: Climate model simulations of the equilibrium climatic response to increased carbon dioxide. *Rev. Geophys.*, **25**, 760–798.
- Schneider, E. K., and J. L. Kinter III, 1994: An examination of internally generated variability in long climate simulations. *Climate Dyn.*, **10**, 181–204.
- , R. S. Lindzen, and B. P. Kirtman, 1997: A tropical influence on global climate. *J. Atmos. Sci.*, **54**, 1349–1358.
- Sela, J. G., 1980: Spectral modeling at the National Meteorological Center. *Mon. Wea. Rev.*, **108**, 1279–1292.
- Shine, K. P., and A. Sinha, 1991: Sensitivity of the Earth's climate to height dependent changes in the water vapor mixing ratio. *Nature*, **354**, 382–384.
- Slingo, J. M., 1987: The development and verification of a cloud prediction scheme for the ECMWF model. *Quart. J. Roy. Meteor. Soc.*, **113**, 899–927.
- Spencer, R. W., and W. D. Braswell, 1997: How dry is the tropical free troposphere? Implications for global warming theory. *Bull. Amer. Meteor. Soc.*, **78**, 1097–1106.
- Sun, D.-Z., and R. S. Lindzen, 1993: Distribution of tropical tropospheric water vapor. *J. Atmos. Sci.*, **50**, 1643–1660.